



Supporting Online Material for

Observed Flow Compensation Associated with the MOC at 26.5°N in the Atlantic

Torsten Kanzow,* Stuart A. Cunningham, Darren Rayner, Joël J.-M. Hirschi, William E. Johns, Molly O. Baringer, Harry L. Bryden, Lisa M. Beal, Christopher S. Meinen, Jochem Marotzke*

*To whom correspondence should be addressed. E-mail: tok@noc.soton.ac.uk (T.K.); jochem.marotzke@zmaw.de (J.M.)

Published 17 August 2007, *Science* **317**, 938 (2007)
DOI: 10.1126/science.1141293

This PDF file includes:

Materials and Methods
SOM Text
Figs. S1 to S3
Tables S1 to S3
References

Supporting Online Material

1. Materials and Methods

1.1 Data Overview, sampling, filtering, statistical significance

The RAPID / MOCHA experiment design has been successfully tested in model studies (*S1*). The simulations suggested that the absolute, zonally-integrated, meridional mid-ocean geostrophic flow across 26.5°N can be recovered successfully by observing density profiles at the western and eastern boundaries of the basin and at both sides of the Mid-Atlantic Ridge. In the simulations the MOC signal is decomposed into northward Gulf Stream transports (T_{GS}) near the western boundary and zonally integrated near-surface Ekman transports (T_{EK}), compensated by mid-ocean geostrophic transports (T_{MO}). This paper follows a similar terminology in describing the observations.

Table S1 together with Fig. 1 give an overview over the data that have been used. The sampling rate of the sensors used to measure temperature, salinity and pressure on the density moorings is 15 minutes. The sensors that acquire bottom pressure have a sampling rate of 10 minutes. The current meters sample at 15 minute intervals. The electromagnetic cable measurements to determine T_{GS} in the Straits of Florida are supplied by NOAA / AOML with daily resolution and are considered to represent daily averages. The same is true for the Quikscat wind stress data provided by CERSAT, IFREMER. For all discussions, time series filtering with a six-pole Butterworth filter is used. For the subsequent discussion the statistical significance of correlations is estimated at a 5 percent error probability, with degrees of freedom derived according to (*S2*). Estimates of variability and uncertainties refer to one standard deviation.

1.2 Computation of internal transports (T_{INT})

To compute T_{INT} , i.e. the section-wide integrated geostrophic transports between the surface and 4820 dbar relative to 4820 dbar, the following steps are taken. Temperature (T), conductivity (C) and pressure (P) time series, acquired at discrete depth levels at the different mooring sites (Fig. 1, Table S1), are in situ-calibrated (11). Then salinity S is computed and S, T and P are two-day low-pass filtered and subsequently interpolated on a half-daily grid. T and S are then vertically interpolated onto a regular 20 dbar pressure grid. The vertical interpolation between the measurement levels uses vertical gradients of T and S as empirical functions of T (12). To compute the western boundary profile, T and S from the moorings WB2, WBH1 and WBH2 have been merged and for the eastern boundary profile moorings EB1, EBH1, EBH2, EBH3, EBH4 and EBH5 have been merged (Fig. 1, Table S1). The merging of the data from different moorings is justified, since densities at the basin margins are sufficient to recover the basin-wide velocity shear (S1). The distribution of the sensors on different moorings “crawling” up the western and eastern continental slopes enables us to keep the area of unobserved bottom triangles small.

At the western and eastern boundaries the uppermost mooring measurements were acquired at 100 and 540 dbar, respectively. To match the coverage of the western boundary, T and S from the eastern boundary are extrapolated from 540 to 100 dbar at each time step as follows. We linearly extrapolate the anomalies up to 240 dbar using the anomalies at 840 and 540 dbars to estimate the gradient and then carry the anomaly at 240 dbar at constant value up to 100 dbar.

From the resulting profiles of density differences between the western and eastern boundary, we compute the geostrophic transport (per unit depth) relative to 4820 dbar, which will be referred to as *internal transport* (T_{INT}) following (11). The internal transport per-unit-depth profiles $T_{INT}(z)$ have

been extrapolated from 100 dbar to the surface at constant value to include the whole water column. The small contribution of transports relative to 1400 m through the 10 km wide section between WB1 and WB2, estimated by direct current meter measurements (rather than density) is added to $T_{INT}(z)$. We choose to do so because the quality of the density measurements at WB1 is poor. As described below, using the relative flow between WB1 and WB2 as a part of $T_{INT}(z)$ allows us to have $T_{INT}(z)$ cover the same set of moorings (or zonal integration scale) as the complementary external transport $T_{EXT}(z)$ (which uses bottom pressure difference between WB1 and WB2).

1.3 Computation of external transports (T_{EXT})

To compute the section-wide integrated external transport fluctuations T_{EXT} from the bottom pressure measurements, the following steps are carried out. The instrumental pressure drift is removed empirically from each time series (S3). The time series are then two-day low-pass filtered and interpolated on a half-daily grid. Finally the fortnightly and monthly tides are removed using a harmonic analysis and the time mean is subtracted (11).

Zonal differences of bottom pressure fluctuations P_{BOT} (time mean has been removed) allow the computation of reference level meridional geostrophic velocity fluctuations (11,12). From these the vertically integrated *external transport* fluctuations $\overline{T_{EXT}^i}$ integrated between two stations i and $i+1$ with water column height H can be obtained as $\overline{T_{EXT}^i} = H^i / (f\rho) [P_{BOT}^{i+1} - P_{BOT}^i]$. $\overline{T_{EXT}^i}$ is computed between any pair of adjacent moorings (i.e., for WB1-WB2, WB2-WBH1, WBH1-WBH2, WBH2-EB1, ...), with ρ and f denoting water density and the Coriolis parameter, respectively. Since H changes from site to site, for each pair of bottom pressure measurements the deeper of the two has

been adjusted to the shallower level to compute zonal pressure differences. Therefore we subtract from the bottom pressure record at the deeper site the relative pressure contribution resulting from density fluctuations below the shallower level, using the corresponding mooring T and S measurements. For the subsequent analysis the coast-to-coast zonal transport integral $\overline{T_{EXT}}$ computed from the sum of the ten station pairs has been used ($\overline{T_{EXT}} = \sum \overline{T_{EXT}^i}$). For the study of the vertical structure of the MOC the transport per-unit-depth profile $T_{EXT}(z)$ needs to be computed. Each of the contributions (derived from the ten station pairs) provide a depth-independent profile by definition. However, the zonally integrated $T_{EXT}(z)$ profile displays depth-dependent fluctuations because the transports between the different station pairs contribute over different depth range (as H changes zonally).

1.4 Other transport components

The fraction of the meridional transport over the continental slope west of WB1 (Fig.1, left) has been estimated by integrating velocities from direct current meter measurements on the moorings WBA, WB0, WB1 (14). Flows in this wedge - hereafter referred to as *western boundary wedge transports* (T_{WBW}) - are dominated by the upper-ocean northward Antilles current (S4) and by the upper and inshore fraction of the southward deep western boundary current (DWBC).

At 26.5°N the northward T_{GS} is topographically confined to the Straits of Florida (Fig. 1). Its temporal evolution has been estimated quasi-continuously over the last 25 years from voltage fluctuations induced on a telephone cable between Florida and the Bahamas (S5). During 2004 there is a two month long gap in T_{GS} from September to October 2004 resulting from damage to the recording facility.

The Ekman transport zonally integrated between the Bahamas and the African coast

$\overline{T_{EK}} = -\int \tau_x /(\rho f) dx$ is estimated from zonal integral of the zonal component of wind stress τ_x

from Quikscat scatterometer measurements (14) .

1.5 Transport per-unit-depth profiles

To be able to define MOC fluctuations, we need to analyse how the meridional transport variability is distributed in the vertical. Therefore profiles of transport per-unit-depth have been computed for all components. For $T_{INT}(z)$, $T_{EXT}(z)$ and $T_{WBW}(z)$ this is straightforward. To obtain $T_{EK}(z)$ we distributed the transport evenly over the top 100 m below the surface. For $T_{GS}(z)$, the transport per-unit-depth was computed by projecting $\overline{T_{GS}}$ onto the first vertical mode of meridional transport per-unit-depth, determined by an empirical orthogonal function analysis of the meridional velocity measurements from 64 historical Pegasus sections across the Straits of Florida (because the telephone cable measurements provide the vertical transport integral, but no information on the vertical distribution). The first mode contains 87 % of the variance. $T_{GS}(z)$ extends from the surface to 780 m.

2. Supporting text

2.1 Error analysis

The errors in $\overline{T_{INT}}$ amount to ± 2.0 Sv, based an error estimate for $\overline{T_{INT}}$ of ± 2.5 Sv for a precursor experiment near 26.5° N (12). There, a lower number of vertical density sampling levels was used, as well as less precise temperature sensors and no conductivity measurements. The

uncertainty in $\overline{T_{EXT}}$ on time scales much shorter than the record length should not exceed ± 1.5 Sv (11). Errors in fluctuations of $\overline{T_{GS}}$ amount to ± 1.0 Sv (S6). Uncertainties of $\overline{T_{EK}}$ and $\overline{T_{WBW}}$ are ± 0.5 Sv and ± 0.3 Sv, respectively, based on comparisons to NCEP/NCAR wind stress and lowered acoustic Doppler current measurements at the western boundary, respectively. This gives an error estimate for the total transport fluctuations of ± 2.6 Sv.

According to simulations using temperature and salinity time series from the EBH4 and EBH5 moorings from the 2005-2006 deployment period, where measurements at 8 levels between 600 dbar and 50 dbar were available, the extrapolation of temperatures and salinities from 540 to 50 dbar at the eastern boundary introduces an additional error to $\overline{T_{INT}}$ of less than ± 0.5 Sv. Assuming this additional uncertainty to be independent from the ± 2.6 Sv uncertainty of the total transport fluctuations results in an overall transport error estimate of ± 2.7 Sv.

To compute MOC fluctuations we have vertically integrated the sum of the transport per-unit depth profiles $T_{INT}(z) + T_{EXT}(z) + T_{WBW}(z) + T_{EK}(z) + T_{GS}(z)$ from 4820 to 1000 dbar. $T_{GS}(z)$ and $T_{EK}(z)$ do not contribute in this layer (see above). From $T_{INT}(z)$ and $T_{EXT}(z)$ only the uncertainty deeper than 1000 dbar has to be taken into account (i.e., about 80 % of their bottom to surface integrated error, or ± 1.6 and ± 1.2 Sv, respectively). Assuming the uncertainties of $T_{INT}(z)$ and $T_{EXT}(z)$ to be independent this gives an overall uncertainty of ± 2.0 Sv. The error contribution of $T_{WBW}(z)$ is negligible in the pressure range under consideration.

2.2 Spectral distribution of transports and their compensation

Variability in both $\overline{T_{INT}}$ and $\overline{T_{EXT}}$ peaks near 20 days and in the 40 - 80 day range, with $\overline{T_{EXT}}$ displaying a slightly larger variance than $\overline{T_{INT}}$ (Fig. S1). This demonstrates that the density field varies substantially on periods shorter than one month ($\overline{T_{INT}}$ fluctuates by ± 5.3 Sv when thirty-day high-pass filtered). The sum of $\overline{T_{INT}}$, $\overline{T_{EXT}}$ and $\overline{T_{WBW}}$, $\overline{T_{EK}}$ and $\overline{T_{GS}}$ (Fig. S1, black line) – hereafter referred to as mid-ocean transport ($\overline{T_{MO}}$) – displays significantly lower variance than either $\overline{T_{EXT}}$ or $\overline{T_{INT}}$ alone, for periods greater than 10 days. The sum of $\overline{T_{EK}}$ and $\overline{T_{GS}}$ – referred to as (surface plus western) *boundary transport* ($\overline{T_{BOUND}}$) – further compensates for $\overline{T_{MO}}$ variability: The sum of all five transport contributions ($\overline{T_{INT}} + \overline{T_{EXT}} + \overline{T_{WBW}} + \overline{T_{EK}} + \overline{T_{GS}} = \overline{T_{MO}} + \overline{T_{BOUND}}$) – referred to as unconstrained total transport - displays a further variance reduction, compared to $\overline{T_{MO}}$, at periods larger than 30 days (Fig. S1, cyan line).

2.3 Filling the gap in $\overline{T_{BOUND}}$

The two-month gap in $\overline{T_{BOUND}}$ would have limited our analysis to a 10 month long record. We fill the gap (dashed part of grey line in Fig. 2b) by means of a linear regression between $\overline{T_{MO}}$ and $\overline{T_{BOUND}}$, namely: $\overline{T_{BOUND}} = -0.81 \times \overline{T_{MO}} + 0.45$. An additional linear trend $a \times t + b$ with $a = 0.066$ Sv/day and $b = 2.2$ Sv over time t is required to match the regression with the original time series at the gap end points.

2.4 The Mid-Atlantic Ridge problem – a crude assessment

We estimate the MOC variability using the eastern-to-western boundary pressure (density) gradients to compute the mid-ocean transport. However, the Mid Atlantic Ridge (MAR) divides the Atlantic into an eastern and a western basin (Fig. S2). Thus, time-variable meridional flows below

the MAR crest in the western and eastern basin are likely be independent from each other, possibly resulting in a time-variable pressure gradient across the MAR. This may limit the validity of our approach in the deep ocean. Here we attempt a crude assessment to what degree pressure gradients across the MAR contribute to the MOC fluctuations.

At 26.5° N the MAR crest height is at about 2500 dbar, located at 44.4° W. Several deep trenches (or fracture zones) with an nearly zonal orientation cut though the MAR and thus allow for a zonal exchange of deep and bottom waters at much greater depths. In the low-latitude North Atlantic major trenches are the Romanche, Vema, Fifteen Twenty and Kane fracture zones, located at roughly 1° N, 11° N, 15° N and 24° N, respectively. All of them have a sill (minimum) depth of at least 3700 dbar (Vema Fracture Zone's sill depth is deeper than 4500 dbar). During the Spring 2004 to Spring 2005 deployment density moorings covering the 2500 – 4820 dbar range have been located on the eastern and western flank of the Mid-Atlantic Ridge near 24.5° N, one at 50° W (MAR1) and the other at 41° W (MAR2), both of which also featuring bottom pressure sensors (Fig. S2 and Table S1).

To assess the influence of the MAR on the MOC variability, we now estimate the deep transports independently for the eastern and western basin between the bottom (4820 dbar) and certain level below the MAR crest. Given the existence of the several deep fracture zones (with Kane Fracture Zone being very close to our section), for simplicity we assume that only below 3700 dbar the MAR needs to be considered a solid meridional boundary (such that no meridional flow occurs between MAR1 and MAR2 below that level). However, at levels shallower than 3700 dbar we consider the MAR permeable (absent) and assume that a pressure gradient between MAR1 and MAR2 balances a geostrophic meridional geostrophic flow between the two sites (Fig. S2).

The following steps are taken to derive the MOC fluctuation including the MAR measurements. We compute the sum of the western basin and eastern basin internal transport profiles $T_{INT}(z)$ relative to 4820 dbar between 3700 and 4820 dbar. For the western basin the densities at WB2, WBH1 and WBH2 provide the western density profile and data at MAR1 the eastern density profile (Fig. S2). For the eastern basin the densities at MAR2 provide the western density profile and data at EB1, EBH1, EBH2, EBH3, EBH4 and EBH5 the eastern density profile. Above 3700 dbar we calculated $T_{INT}(z)$ relative to 3700 dbar only using data from the eastern and western boundary of the Atlantic. To join $T_{INT}(z)$ above and below 3700 dbar together, at each time step the transport value at 3700 dbar of the deep profile is added as an offset to the profile above 3700 dbar.

To take into account the presence of the MAR in the external transport $T_{EXT}(z)$ calculations, the contribution between WBH2 and EB1 requires modification (west of WB2 and east of EB1 no modification is required). We now compute the sum of the independent $T_{EXT}(z)$ contributions of the western basin (WBH2 – MAR1) and the eastern basin (MAR2 – EB1) in the 0 – 4820 dbar layer. To this we add the $T_{EXT}(z)$ contribution over the MAR (MAR1 – MAR2) in the 0 – 3700 dbar layer (since we assume now flow to occur between the two moorings below 3700 dbar). To achieve this the bottom pressure measurements at MAR1 and MAR2 are adjusted to the 3700 dbar level by subtracting the density-related pressure fluctuations between the 3700 dbar and the bottom. The remaining transport components required to derive MOC fluctuations ($T_{WBW}(z)$, $T_{EK}(z)$, $T_{GS}(z)$) are not subject to modifications.

The MOC timeseries (defined the same way as in Fig. 4) with and without taking the presence of the MAR into account (red and black lines in Fig. S3, respectively) look almost identical. Their difference (green line) varies by ± 1.1 Sv, while the MOC timeseries varies by ± 5.7 Sv. Our crude assessment confirms that role of the MAR on the time scales considered here is rather small

but certainly not negligible. This confirms our initial approach not to include the MAR measurements into our initial MOC calculations (Figs. 2-4 and S1). Also, it is difficult to attribute the transport difference (green line in Fig. S3) entirely to time variable pressure gradients across the MAR, as explained below.

When computing the deep transports below 3700 dbar independently for the western and eastern basin, the transport below 3700 dbar in a 950 km wide section between the two MAR moorings remains unobserved (in the wedges between the MAR1 and MAR2 and the MAR bathymetry, Fig. S2). It is reasonable to assume that one of the dominant time-variable transport signals in the deep basin interior (on the time scales considered) arise from westward propagating Rossby waves (11). While the net effect of Rossby waves on the MOC - as long as they reside in the basin interior - is negligible, leaving that area unobserved may introduce a net transport signal (e.g. caused by Rossby waves propagating into or out of this shadow zone), that could be misinterpreted as time-variable MOC signals.

Therefore the interpretation of the calculations including the measurements on both MAR flanks is delicate and we emphasize that the assessment of the role of the MAR presented here is rather crude. A more in-depth study is required that attempts to take into account the transports in the wedges of either flank of the MAR. Even though we have only seen a small change in MOC variability after taking into account the presence of the MAR, we think that long-term measurements on the MAR flanks are required. The influence of the Antarctic Bottom Water (AABW) – representing the densest and thus deepest water mass in the Atlantic – is most clearly detectable on the western MAR flank, with the abyssal isotherms rising by several hundred meters along 26.5°N from the western boundary towards the MAR. The AABW has been shown to undergo a long-term warming since the 1970s in the South Atlantic (S7). Thus, there is potential for long-term transport changes in the deepest layers of the water column.

3.Supporting Figures

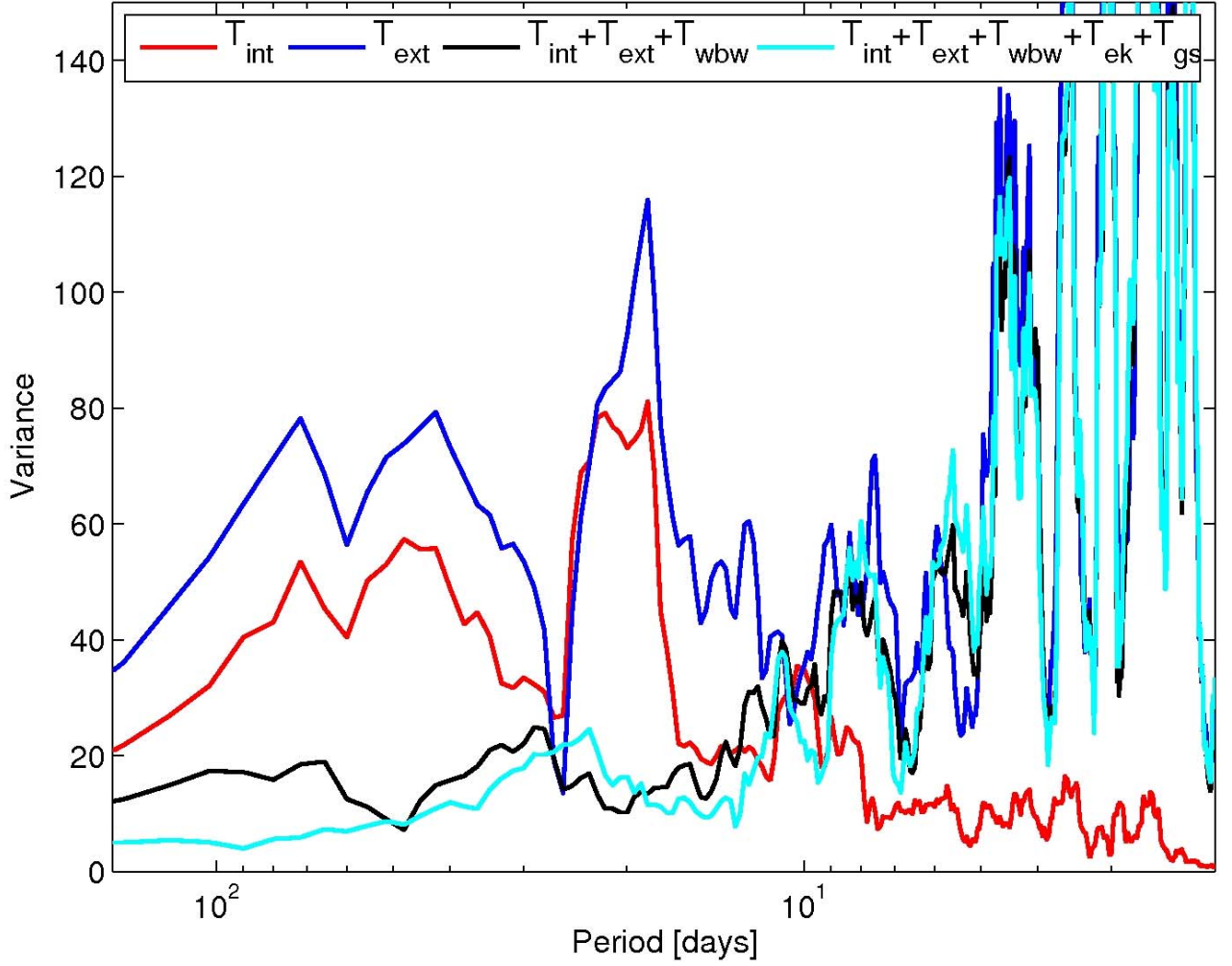


Fig. S1: Variance conserving spectra of transports based on the time series in Fig. 2a. The red, blue, black and cyan lines denote internal $\overline{T_{INT}}$, external $\overline{T_{EXT}}$ and mid-ocean $\overline{T_{INT}} + \overline{T_{EXT}} + \overline{T_{WBW}}$ transports and the sum of all components $\overline{T_{INT}} + \overline{T_{EXT}} + \overline{T_{WBW}} + \overline{T_{EK}} + \overline{T_{GS}}$, respectively. For the

computation of the cyan line, the two month gap in $\overline{T_{GS}}$ has been filled by a linear interpolation.

That means, that high-frequency variability in $\overline{T_{GS}}$ is artificially lowered to a certain degree.

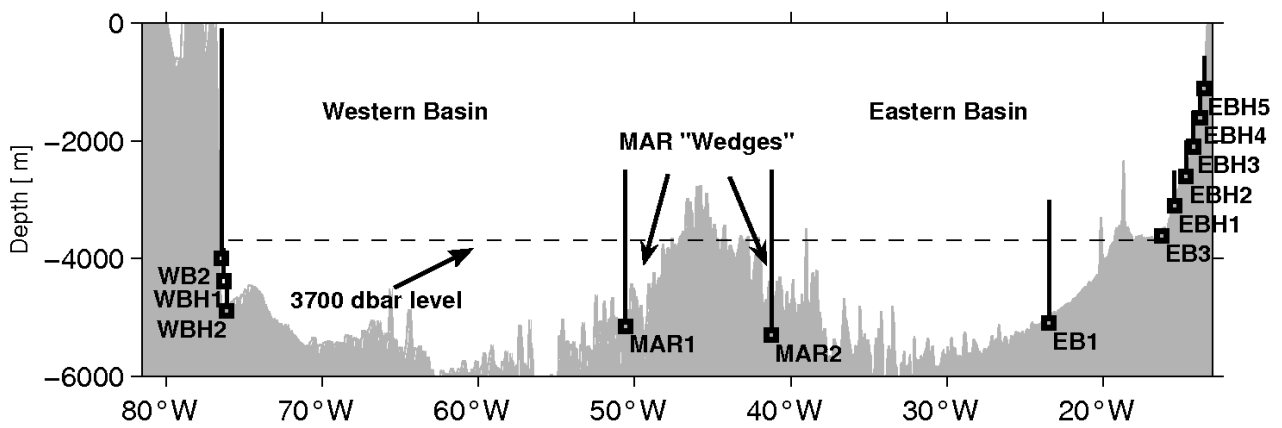


Fig. S2: Distribution of the moorings measuring density (vertical lines) and bottom pressure along 26.5°N. We refer to the areas west and east of the crest of the Mid-Atlantic Ridge as western and eastern basin, respectively. The areas deeper than 3700 dbar between MAR1 and the MAR bathymetry as well as between the MAR bathymetry and MAR2 are referred to as MAR wedges.

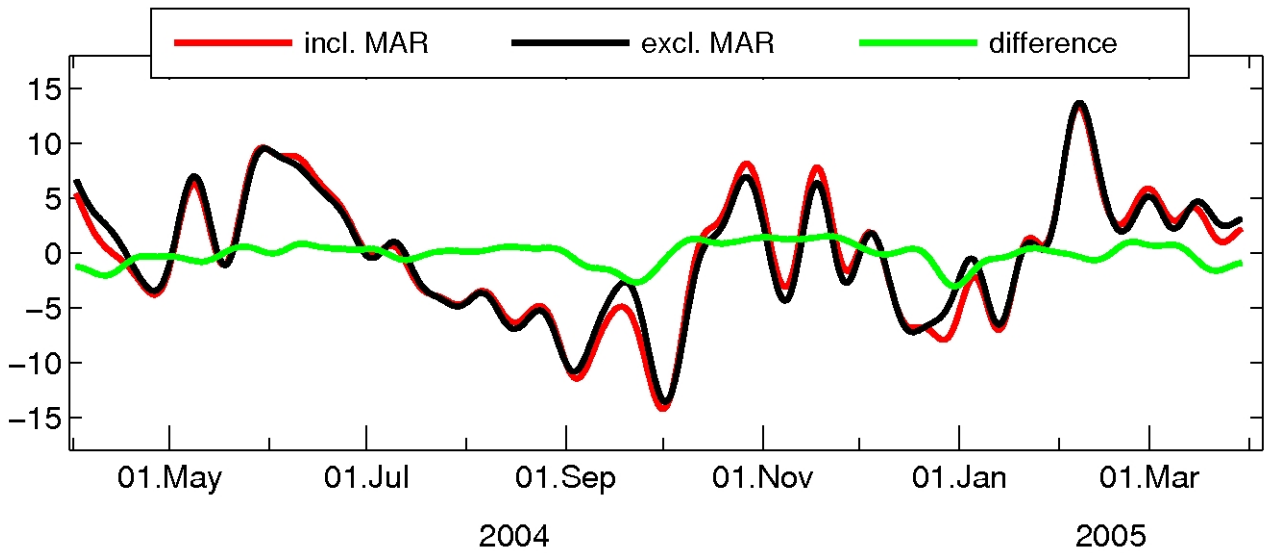


Fig. S3: Transports between 1000 and 4820 dbar (or MOC fluctuations as defined in Fig. 4)

including and excluding the density and bottom pressure fluctuations on both flanks of the Mid-Atlantic Ridge are shown as red and black lines, respectively. Their difference is displayed as green line.

Mooring	Longitude	T/S Range	T/S levels	BPR	Current Meter Range	Current Meters Levels
WBA	76° 52.8'	---	---	---	0 - 400	1*
WB0	76° 50.5'	---	---	---	0 - 800	4*
WB1	76° 48.8'	---	---	x	50 - 1400	9
WB2	76° 44.5'	100 - 3795	14	x	150 – 2000	5
WBH1	76° 41.9'	3875 - 4315	5	x	---	---
WBH2	76° 36.0'	4370 - 4810	5	x	---	---
EB1	23° 26.9'	2895 - 4930	5	x	---	---
EB3	16° 13.8'	---	---	x	---	---
EBH1	15° 25.0'	2570 - 2780	2	x	---	---
EBH2	14° 41.0'	2058	1	x	---	---
EBH3	14° 12.3'	1547 - 1981	5	x	---	---
EBH4	13° 47.3'	1044 - 1475	5	x	---	---
EBH5	13° 31.2'	530 - 962	5	x	---	---
MAR1	50° 34.2'	2400 - 5070	6	x	---	---
MAR2	41° 12.9'	2550 - 5250	6	x	---	---

(*) The shallowest instrument level was occupied by a broadband acoustic Doppler current profiler (ADCP).

Table S1: Overview over mooring data used in this study. T/S range [dbar] and T/S levels indicate the pressure range and the number of levels where temperature and salinity were measured. BPR

denotes at which sites bottom pressure measurements were available. Current meter range [dbar] and current meter levels refer to the pressure range and the number of levels where direct velocity measurements were taken.

Synonym	Full name	Meaning	Technique
T_{GS}	Gulf Stream Transport	Transport through Straits of Florida	Electromagnetic cable measurement
T_{EK}	Ekman Transport	Meridional wind driven transport between Bahamas and African coast	Space borne scatterometry
T_{INT}	Internal Transport	Geostrophic transport rel. to 4820 dbar from Bahamas (WB1) to Africa	Moored temperature and salinity
T_{EXT}	External Transport	Reference level geostrophic transport contribution from Bahamas (WB1) to Africa	Moored bottom pressure
T_{WBW}	Western Boundary Wedge Transport	Transport over Bahamian continental slope west of WB1	Moored current and bottom pressure
T_{MO}	Mid-Ocean Transport	$T_{INT} + T_{EXT} + T_{WBW} =$ geostrophic transport between Bahamas and Africa	see T_{INT} , T_{EXT} , T_{WBW}
T_{BOUND}	Boundary Transport	$T_{EK} + T_{GS} =$ transport in surface (Ekman layer) and western boundary layer (Gulf Stream)	see T_{EK} , T_{GS}

Table S2: Overview of the different transport synonyms, definitions and measurement techniques

Case	constrained variables	variables considered constant
total geostrophic	$T_{INT} + T_{WBW} + T_{GS}$	T_{EK}
total	$T_{INT} + T_{WBW} + T_{EK} + T_{GS}$	None

Table S3: Summary of constrained MOC contribution shown in Fig. S2

5. Supporting references and notes

- S1. Hirschi, J., Baehr, J., Marotzke, J., *Geophys. Res. Lett.*, **30**, 1443 (2003).
- S2. Davis, R.E., *J. Phys. Oceanogr.* **6**, 249 (1976).
- S3. Watts, D.R., Kontoyiannis, H., *J. Atm. Oceanic Tech.* **7**, 296 (1990).
- S4. Lee, T.N., W.E. Johns, R. Zantopp, E.R. Fillenbaum, *J. Phys. Oceanogr.* **26**, 962 (1996).
- S5. Baringer, M.O., J.C. Larsen *Geophys. Res. Lett.* **28**, 3179 (2001).
- S6. Larsen, J.C., *Philosoph. Trans. Royal Soc. London A* **338**, 169 (1992).
- S7. Zenk, W., A. Sokov, T.J. Müller, *Clivar Exchanges* **26**, 24 (2003).